Robust Multiphase-Split Calculations Based on Improved Successive Substitution Schemes

M. Jex[1], J. Mikyška[1], and A. Firoozabadi[2]*

[1]Department of Mathematics, Czech Technical University in Prague
[2]Chemical and Biomolecular Engineering Department, Rice University

Summary

Successful large-scale compositional reservoir simulations require robust and efficient phase-split calculations. In recent years, there has been progress in three-phase-split calculations. However, there may be convergence issues when the number of equilibrium phases increases to four. Part of the problem is from the poor initial guesses. In phase-split computations, the results from stability provide good initial guesses. Successive substitution (SS) is a key step in phase-split calculations. The method, if efficient, can provide good initial guesses for the final step, the Newton method that has a rapid rate of convergence. In this contribution, we present a robust algorithm with high efficiency and robustness in phase-split calculations in two, three, and four phases. We find that a key step is the SS. The convergence may even be very slow away from the critical point and phase boundaries. A modified SS is used which may reduce the number of iterations many times. In the course of this investigation, we observe some regions often inside the phase envelopes (far from the phase boundary or critical points) with a very high number of SS iterations. The adoption of the improved SS iterations leads to a significant speedup of the multiphase-split computations. In some mixtures, the average reduction is more than 70%.

Introduction

In recent years, there has been an increasing interest in large-scale compositional simulations in various fields for oil recovery and CO_2 sequestration. In the injection of CO_2, one needs a robust and efficient algorithm for the phase splitting of various species in different phases. The standard procedure to solve the problem consists of phase stability testing and multiphase-split calculations. Typically, we proceed in several steps. First, the stability of a mixture is assessed. If the mixture is unstable, then a new phase is added, and we move to multiphase-split computations where the state found in phase stability is used to construct an initial approximation. In phase-split computations, the usual approach is to proceed from the SS to the Newton-Raphson (NR) method. The closer the initial guess is to the true solution, the faster is the convergence to the true solution. The SS method is computationally less expensive than the NR method. A major strategy is having SS converge sufficiently close to a solution and only then switch to NR, which will finalize the computation. We start the computations with stability, and then after every phase-split computation, we examine the stability of one of the phases. If the phase is found unstable, we increase the number of phases and continue the phase-split calculation. The higher phase split is repeated until the phases are stable. Several mathematically challenging problems are to be addressed in the process of solving this complex problem.

There are a number of solutions to the phase stability testing. We have adopted the local minimization technique for the optimization of the tangent plane distance (TPD) function (Michelsen 1982a). A mixture is found unstable if there is a local minimum of the TPD function with a negative value. Multiple initial guesses are needed to ensure the correct assessment of stability. If the mixture is unstable with multiple negative local minima, we continue with the phase-split calculation using the initial estimate from stability with the lowest value of the TPD function. In three- and four-phase-split computations, when phase-split computations fail with the lowest TPD value, we may use the initial guess from the next lower TPD to reinitialize the corresponding two- or three-phase split.

The first step in the phase-split calculation is solving the Rachford-Rice (RR) equation(s). Depending on the number of phases, we use either the bisection method (Mikyška 2023) often combined with NR (in two phases) or the NR method with line search (Okuno et al. 2010) in three and four phases. Then, we usually continue by using SS to obtain a sufficiently accurate solution. In our experience, the converged solution from SS is often close enough to the true solution and the subsequent NR method often converges in one or two iterations.

Despite extensive published reports on the phase-split calculations, there are few reports that provide the number of iterations in the form of a map with a number of iterations in SS or NR. Usually, central processing unit (CPU) times or the number of iterations in isolated cases are presented (Paterson et al. 2018; Imai et al. 2019; Chen et al. 2023).

Michelsen in his pioneering work (Michelsen 1982a, 1982b) presents an algorithm for phase-stability and phase-split computations. He suggests the stability computation as a first step for the phase-split computations. Then, he discusses the effect of stability on the phase-split computations (SS and NR). The solution to the RR equation was presented earlier by Rachford and Rice (1952), where they use the bisection method. In three- and four-phase-split computations, a more advanced approach such as the NR method with line search (Okuno et al. 2010) or trust region method (Pan et al. 2021) will be required.

Various authors have used alternatives including the reduction methods (Petitfrere and Nichita 2015), globally convergent Newton optimization such as line search (Michelsen 1982b), and the trust region (Michelsen 1993; Petitfrere and Nichita 2014; Pan et al. 2019) as opposed to the classical Michelsen's approach in which he suggests the SS followed by the NR (Michelsen 1982b). Petitfrere and Nichita (2014, 2015) and Pan et al. (2019) propose to use the trust-region methods in phase stability testing, multiphase equilibrium calculations, and RR system solutions as a part of a sequential procedure, in which SS iterations are followed by NR iterations, and in case

*Corresponding author; email: abbas.firoozabadi@rice.edu

Original SPE manuscript received for review 4 December 2023. Revised manuscript received for review 21 February 2024. Paper (SPE 219490) peer approved 22 February 2024. Supplementary materials are available in support of this paper and have been published online under Supplementary Data at https://doi.org/10.2118/219490-PA. SPE is not responsible for the content or functionality of supplementary materials supplied by the authors.

of divergence, NR iterations are switched to the trust region method. In this work, we show that the same degree of robustness and efficiency can be attained within the framework of the SS + NR approach in both three-phase and four-phase splits.

We believe in the simplicity of the conventional approach and its powerful features and adapt it in this work. We discuss the essential details in maps of independent computations for a large number of mixtures to give a clear picture of basic issues that may not have been discussed in the past for two-, three-, and four-phase-split computations. A clear picture will then evolve. In the past, an increase in the number of iterations has been reported close to the phase boundary and near the critical points (Petitfrere and Nichita 2014; Trangenstein 1987). In this work, we have found a high number of iterations that are neither in the proximity of the phase boundaries nor near critical points.

We have introduced a modification to the conventional SS algorithm (Mehra et al. 1983; Heidemann and Michelsen 1995) to reduce the number of SS iterations significantly. Heidemann and Michelsen (1995) introduced a constant damping factor to update K values which improves the stability of the algorithm. Mehra et al. (1983) introduced an update of this damping factor in each iteration and discussed the effect on the number of iterations in two-phase split. We extend this approach to three- and four-phase systems. Other acceleration techniques have been suggested by Risnes (1981) and Perschke (1988), which will be covered later in this work.

Overall Phase-Split Algorithm

Our goal is to predict mixture splitting into multiple phases (number of phases and their composition). One provides pressure, temperature, and molar composition of a mixture, physical parameters of components in the mixture [we use the Peng-Robinson equation of state (Peng and Robinson 1976)]. Outputs are the number of phases, phase molar fractions, and composition of the phases. **Fig. 1** shows the flow chart of a multiphase-split calculation. In most cases, K values related to the lowest TPD are the best initial guess. However, occasionally in three- or four-phase splits, the values converge to a nonphysical solution with a negative value of phase molar fractions. In this case, we return to two- or three-phase splits, respectively, and perform the phase-split calculations again with K values corresponding to the next lower TPD value. The procedure is similar to that of Pan et al. (2019), but with a slight modification. First, we perform two-phase split with the K values corresponding to the lowest negative TPD in single-phase stability testing. If the three-phase split fails, another two-phase split is performed. We start the second two-phase split using the K values associated with the next lowest negative TPD in the two-phase stability testing. Two-phase stability testing and three-phase split (if required) then follow. Similarly, if the four-phase split

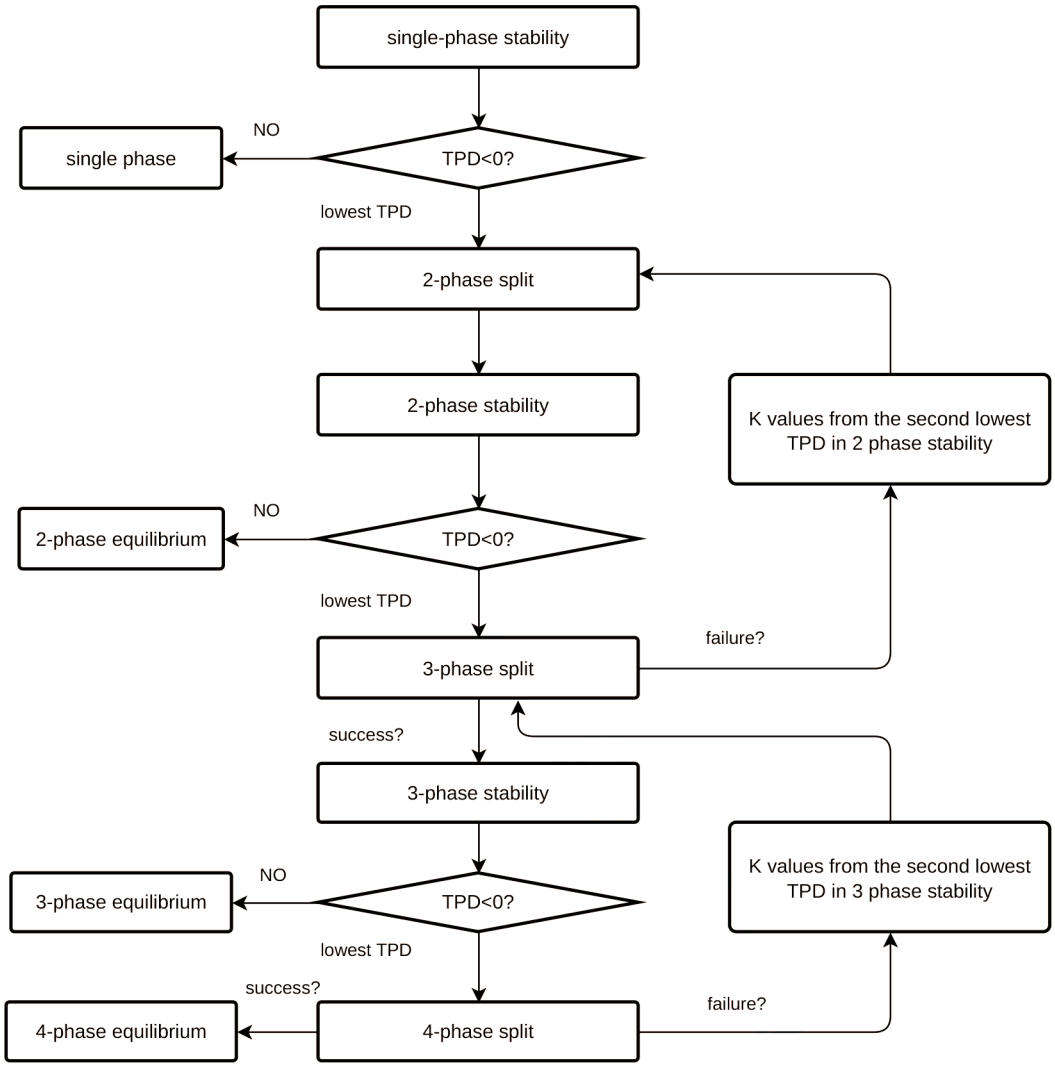

Fig. 1—Flow chart of the computational algorithm.

fails, another three-phase split is performed using the K values associated with the next lowest negative TPD in the three-phase stability testing.

Phase Stability Testing

As stated above, the first step in the phase-split calculations is phase stability testing. We adopt the local minimization approach (Hoteit and Firoozabadi 2006), with multiple initial guesses (Li and Firoozabadi 2012) to ensure convergence to nontrivial minima. Additionally, we include other initial guesses for CO_2 and H_2O when they have a high concentration in some mixtures as suggested by Imai et al. (2019), Li and Li (2019), and Connolly et al. (2019):

$$K_i^{\text{stab}}(\mathbf{x}^*) = \left[K_i^{\text{Wilson}}, 1/K_i^{\text{Wilson}}, \sqrt[3]{K_i^{\text{Wilson}}}, \sqrt[3]{1/K_i^{\text{Wilson}}}, K_i^{\text{ideal}}, K_i^{\text{pure}}, K_i^{\text{CO}_2}, K^{\text{H}_2\text{O}}\right] \quad i = 1, ..., n, \tag{1}$$

where $\mathbf{x}^*$ is a vector of component mole fractions in the test phase, i is the component index, and n is the number of components. The Wilson equilibrium ratios are given by

$$K_i^{\text{Wilson}} = \frac{P_{c,i}}{P} \exp\left[5.37(1+\omega_i)\left(1 - \frac{T_{c,i}}{T}\right)\right], \quad i = 1, ..., n, \tag{2}$$

where T_c, P_c, and ω are the critical temperature, critical pressure, and acentric factor, respectively. The ideal equilibrium ratios are given by (Imai et al. 2019):

$$K_i^{\text{ideal}} = \varphi_i(\mathbf{x}^*), \quad i = 1, ..., n, \tag{3}$$

where x_i^* is the mole fraction and $\varphi_i(\mathbf{x}^*)$ is the fugacity coefficient of component i. Imai et al. (2019) have suggested the following initial guesses for high-content CO_2 mixtures:

$$K_i^{\text{CO}_2} = \frac{0.95}{x_i^*}, \quad K_l^{\text{CO}_2} = \frac{0.05}{(n-1)x_l^*}, \tag{4}$$

where i is the CO_2 component and $l \neq i$ is the rest of the components. Li and Li (2019) have suggested the following expression for high-H_2O concentration mixtures:

$$K_i^{\text{H}_2\text{O}} = \frac{1 - 10^{-15}}{x_i^*}, \quad K_l^{\text{H}_2\text{O}} = \frac{10^{-15}}{(n-1)x_l^*}, \tag{5}$$

where i is the H_2O component and $l \neq i$ is the rest of the components. Connolly et al. (2019) have also suggested a similar expression with a different exponent (i.e., 10^{-3} instead of 10^{-15}). Li and Firoozabadi (2012) suggested the following expression:

$$K_i^{\text{pure}} = \frac{0.99}{x_i^*}, \quad K_l^{\text{pure}} = \frac{0.01}{(n-1)x_l^*}, \tag{6}$$

with n initial guesses where component i is treated as a pure component and $l \neq i$ is the rest of the components. In a local approach, if we detect a local minimum of the TPD function with a value less than -10^{-7}, the mixture is unstable, and phase-split calculations can be conducted. Otherwise, we end the computation. The reduced molar Gibbs free energy TPD function (Firoozabadi 2016; Michelsen 1982a) is given by

$$\text{TPD}^*(\mathbf{x}) = 1 + \sum_{i=1}^{n} x_i[\ln(\varphi_i(x)) + \ln x_i - \ln(\varphi_i(\mathbf{x}^*)) - \ln x_i^* - 1], \tag{7}$$

where $\mathbf{x}$ is the trial phase composition. We use the local minimization algorithm through the quasi-Newton method with Broyden-Fletcher-Godfarb-Shanno (BFGS) update (Hoteit and Firoozabadi 2006). The main difference from the conventional Newton method is in the computation of the Hessian matrix. The details of the approach can be found in Hoteit and Firoozabadi (2006). Based on some 150,000 independent phase-split computations, the CPU time in stability calculations is close to the phase-split calculations in two-phase state. In three- and four-phase split, stability CPU time is less. The CPU time comparison is presented in Section S-1 of the Supplementary Material. In many problems in reservoir simulations, there is much less need for stability computations, and therefore phase-split computations will take up most of the computational time.

Solution of the RR System of Equations

In two phases, the RR equation can be solved by the simple bisection method, possibly followed by NR. In three and four phases, there are systems of two and three RR equations, respectively. Using the method from Okuno et al. (2010), this problem can be reformulated as a convex minimization problem:

$$\text{Minimize} \quad F = \sum_{i=1}^{n}(-x_i^* \ln|t_i|) \quad \text{s.t.} \quad \boldsymbol{\alpha}_i^T \mathbf{v} \leq h_i, \tag{8}$$

where $x_i^* = \sum_{j=1}^{p} v_j x_{j,i}^*$, $\boldsymbol{\alpha}_i \in \mathbb{R}^n$, $\alpha_{i,j} = 1 - K_{j+1,i}$, $j = 1, ..., p-1$, $t_i = 1 - [\sum_{j=2}^{p}(1 - K_{j,i})v_j]$, $h_i = \min\{1 - x_i^*, \min_j\{1 - K_{j,i}x_i^*\}\}$, and $K_{j,i} = x_{j,i}/x_{1,i}$, where p is the number of phases in the phase split and $\mathbf{v}$ is the molar fraction of the phases. The index 1 represents the reference phase. The $\nabla F = 0$ is the RR system of equations. Therefore, the solution of the RR system of equations is equivalent to finding

the stationary point of function F. The algorithm modifies the Newton step with the line search technique, and as a consequence, it is robust. The algorithm can be summed up in the following steps.

1. An initial estimate of $\mathbf{v}$ values is generated as a mean of vertices of an intersection of $S = \{\mathbf{v}, \boldsymbol{\alpha}_i^T \mathbf{v} \le h_i,\ i = 1, ..., n\}$ and $P = \{\mathbf{v}, \mathrm{v}_j \ge 0,\ j = 1, ..., p\}$.
2. Calculate the gradient of convex function F.
3. Calculate the Hessian matrix of F and solve the system of equations to obtain Newton's direction $d^{(k)} = -(\nabla^2 F^{(k)})^{-1} \nabla F^{(k)}$, where (k) is the iteration number and

$$\nabla F_j = \sum_{i=1}^{n} \frac{(1 - K_{j+1,i}) x_i^*}{t_i} \quad j = 1, ..., p-1, \tag{9}$$

$$(\nabla^2 F)_{j,m} = \sum_{i=1}^{n} \frac{(1 - K_{j+1,i})(1 - K_{m+1,i}) x_i^*}{t_i^2} \quad j, m = 1, ..., p-1. \tag{10}$$

4. Calculate the maximum feasible step size $\lambda_{\max} = \min_i\{(h_i - \boldsymbol{\alpha}_i^T \mathbf{v}^{(k)})/(\boldsymbol{\alpha}_i^T d^{(k)}) : \boldsymbol{\alpha}_i^T d^{(k)} > 0\}$, if $\lambda_{\max} \ge 1$, then $\lambda_{\max} = 1$.
5. Modify step size $\lambda^{(k)}$ from the line search technique. $\lambda_{\max} \ge \lambda^{(k)} \ge 0$, i.e., find $\lambda^{(k)} = s\lambda_{\max}$ such that $g(s) = F(\mathbf{v} + s\lambda_{\max} d)$ is minimum as a function of $s \in (0, 1)$.
6. Update $\mathbf{v}^{(k+1)} = \mathbf{v}^{(k)} + \lambda^{(k)} d^{(k)}$.
7. Check whether the norm of the gradient is less than a specified tolerance. If yes, then stop, else increase k and go back to Step 2. Using this approach, the system of the RR equations is solved in less than eight iterations (usually four to six) in all mixtures investigated in this work. This method is only used in the beginning of the phase-split calculation because, at that time, we do not have a good initial estimate of $\mathbf{v}$. Later in the algorithm, the conventional NR method can be used.

Phase-Split Calculations

From stability testing, the composition of the new phase provides the initial guess for phase-split calculations. In two-phase split, the initial guess is complete from the stability analysis. For three- and four-phase split, there is a need for an additional set of one or two initial guesses of K values, respectively. These initial guesses can be from a previous phase-split calculation. For an initial guess for the second K value set in three-phase split, we use the K values from two-phase split, and in the four-phase, we use the two sets of K values from three-phase split. The initial guess for phase mole fractions $\mathbf{v}$ is computed from the RR system using the initial guess for K values. Traditionally, the combination of SS and NR is used in phase-split calculations. To start SS, one needs an initial guess for phase fractions $\mathbf{v}$, which is obtained by solving the RR system of equations. When we have initial guesses for our variables, we can move to SS (first-order method). The SS has the following structure.

1. The initial guess for K values is from the stability testing.
2. Solve the RR system of equations for $\mathbf{v}$.
3. Calculate mole fractions of every component in every phase and also the compressibility factors (using the equation of state with the new values of the mole fractions):

$$x_{1,i} = \frac{x_i^*}{1 + \sum_{j=2}^{p} v_j (K_{j,i} - 1)}, \quad x_{m,i} = K_{m,1} x_{1,i}, \quad m = 2, ..., p. \tag{11}$$

4. Calculate fugacity coefficients of all components in all phases.
5. Update equilibrium ratios $\ln K_{j,i}^{(k+1)} = \ln K_{j,i}^{(k)} - \ln(f_{j,i}^{(k)}/f_{1,i}^{(k)}), \quad i \in \{1, ..., n\}$ and $j \in \{2, ..., p\}$.
6. Test convergence criteria. In our work, we stop the iterations if $\max(|\ln \mathbf{K}^{(k)} - \ln \mathbf{K}^{(k+1)}|_\infty, |\mathbf{v}^{(k)} - \mathbf{v}^{(k+1)}|_\infty) < 10^{-7}$. If the convergence criterion is not met, Steps 2–6 are repeated until convergence or the maximum number of iterations is reached.

After the SS step converges, the NR method (Firoozabadi 2016) is used to finalize the solution to a precision of 10^{-8}, i.e., $\max(|\ln \mathbf{K}^{(k)} - \ln \mathbf{K}^{(k+1)}|_\infty, |\mathbf{v}^{(k)} - \mathbf{v}^{(k+1)}|_\infty) < 10^{-8}$. Usually, only one or two iterations are needed as we already have a good initial guess from the SS method.

Improvement in the SS. As we will present later, there are unexpected regions where the SS has very slow convergence. We modify the SS by introducing a step size correction factor. A significant improvement in the speed of convergence can be achieved. Step 5 of SS is improved (Mehra et al. 1983) as follows:

$$\ln K_{j,i}^{(k+1)} = \ln K_{j,i}^{(k)} - \mathbf{m}^{(k)} \ln \frac{f_{j,i}^{(k)}}{f_{1,i}^{(k)}}, \tag{12}$$

where parameter $\mathbf{m}^{(k)}$ (step size correction factor) has a significant effect on convergence speed. In the conventional SS method, $\mathbf{m}^{(k)} = 1$. When the parameter $\mathbf{m}^{(k)} > 1$, on average, convergence speeds up. This is analogous behavior with successive overrelaxation variants of the Gauss-Seidel method for solving a linear system of equations (Shima et al. 1999). The major improvement is from taking a similar approach as in Mehra et al. (1983) in the two-phase split. The parameter $\mathbf{m}^{(k)}$ is changed in each iteration. In the improved SS, we update the parameter $\mathbf{m}^{(k)}$ as follows: $\mathbf{m}^{(k)} = \min\{m_j^{(k)}\}, \quad j = 2, ..., p$, where

$$m_j^{(k)} = |[(g_j^{(k-1)})^T \boldsymbol{U}_j^{-1} g_j^{(k-1)} / ((g_j^{(k-1)})^T \boldsymbol{U}_j^{-1} (g_j^{(k-1)} - g_j^{(k)}))] m_j^{(k-1)}|, \quad j = 2, ..., p. \tag{13}$$

Here $g_j^{(k)} \in \mathbb{R}^n$, $g_{j,i}^{(k)} = f_{j,i}^{(k)}/f_{1,i}^{(k)}$, $U_{j,i,l}^{-1} = (v_j v_1)(x_{j,i} x_{1,i}/x_i^*)(\delta_{il} + (x_{j,l} x_{1,l})/(D_j x_l^*))$, $i, l = 1, .., n$, $D_j = 1 - \sum_{i=1}^{n} (x_{j,i} x_{1,i}/x_i^*)$, δ is the Kroneker delta, and $m_j^{(1)} = 1$. In two-phase split ($j = 2$), $\mathbf{m}^{(k)} = m_2^{(k)}$. In three- and four-phase splits, we have multiple sets of $\mathbf{K}$ values. We compute $m_j^{(k)}$

for each of those vectors and then use the minimum as a universal factor. For instance, in the four-phase split, $\mathbf{m}^{(k)} = \min\{m_2^{(k)}, m_3^{(k)}, m_4^{(k)}\}$. In some iterations, parameters $m_j^{(k)}$ may become large. In the case of $|m_j^{(k)} \ln(f_{j,i}^{(k)}/f_{1,i}^{(k)})| \geq L$, we use $m_j^{(k)} = 1$, where $L = 0.1$ in two- and three-phase splits and $L = 0.01$ in four-phase split. We have examined different caps for $\mathbf{m}^{(k)}$ (i.e., 5, 2, and 1.2) in Sections S-2 and S-3 of the Supplementary Material. The algorithm for limiting $\mathbf{m}^{(k)}$ is as follows:

1. In the first iteration, $m_j^{(1)} = 1, \quad j = 2, ..., p$.
2. In subsequent iterations, calculate $m_j^{(k)}$ for $j = 2, ..., p$ from Eq. 13.
3. If $|m_j^{(k)} \ln f_{j,i}^{(k)}/f_{1,i}^{(k)}| \geq L$ for any $j = 2, ..., p$ then $m_j^{(k)} = 1$.
4. $\mathbf{m}^{(k)} = \min\{m_2^{(k)}, m_3^{(k)}, m_4^{(k)}\}$.

We have carried out extensive stability and phase-split calculations in eight different fluid systems. In Examples 1–3, in some of the regions, there are four phases. The maximum number of phases in the rest of the examples is three.

Examples

In the following, we present the performance of the algorithm outlined above for a large group of examples from the literature. Mixtures are mainly hydrocarbons with various nonhydrocarbons such as H_2O, H_2S, N_2, and CO_2. In all the examples, we use the Peng-Robinson equation of state. We cover the PT/cP spaces (c is the composition space). In all mixtures, our calculated phase envelopes are consistent with the literature. In the first example, we provide maps for both algorithms (conventional and improved SS). In the rest, we only present the results for the improved algorithm. A summary of the number of SS and NR iterations in phase split in two-, three-, and four-phase states is presented in Section S-4 of the Supplementary Material.

Example 1: Four-Phase Split. In the first example, phase stability and phase split of an eight-component mixture (BSB oil) from Imai et al. (2019) are investigated over a wide space. We conduct 10,000 independent phase stability and phase-split calculations. The physical properties of various components in the mixture are presented in **Table 1,** where k_{il} is the interaction coefficient between components i (in the column) and l. The mixture composition is investigated in a 100×100 grid for the mixing molar fraction of CO_2 in the range of 0.4–0.95, pressure P in the range of 75–95 bar and $T = 313.71$ K. The total number of iterations and number of phases in both conventional and improved algorithms are depicted in **Fig. 2. Fig. 2c** clearly shows a very high number of iterations in SS, in excess of 1000, in the middle of the four-phase envelope. This observation is different from the literature in that the number of SS iterations increases close to the critical point and phase boundaries (Petitfrere and Nichita 2014; Trangenstein 1987). **Figs. 3 and 4** present the number of iterations in the two-, three-, and four-phase-split calculations in both conventional and improved algorithms. **Fig. 4** shows a high number of SS iterations far away from the phase envelope (in the middle of the four-phase envelope) and also in the region on the top left of the four-phase boundary. There is a significant reduction in the number of SS iterations by modifying the algorithm as **Fig. 4** reveals.

Component	T_c (K)	P_c (bar)	ω	CO_2 k_{il}	H_2O k_{il}	x_i^*
H_2O	647.30	220.89	0.3440	0.095	0.0	0.3000
CO_2	304.20	73.76	0.2250	0.0	0.095	0.0236
C_1	160.00	46.00	0.0080	0.45	0.055	0.0603
C_{2-3}	344.20	44.99	0.1305	0.5	0.055	0.1052
C_{4-6}	463.22	34.00	0.2407	0.5	0.055	0.1170
C_{7-15}	605.75	21.75	0.6177	0.5	0.105	0.2313
C_{16-27}	751.02	16.54	0.9566	0.5	0.105	0.1128
C_{28+}	942.48	16.42	1.2683	0.5	0.105	0.00499

Table 1—Relevant physical parameters and data: Example 1.

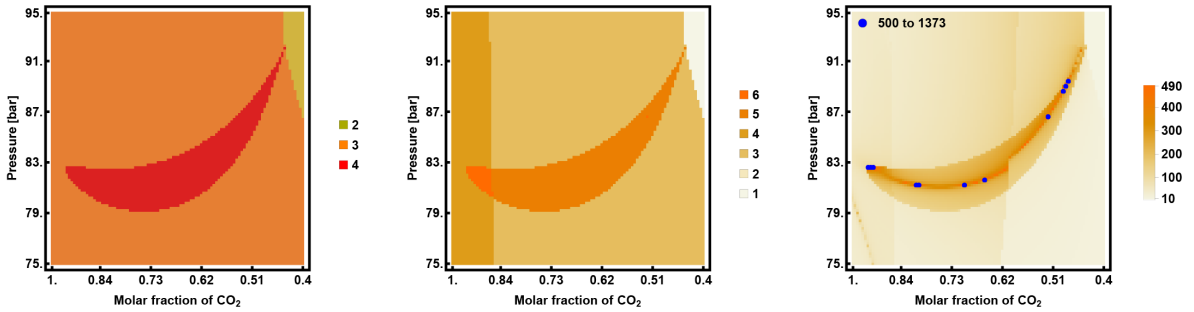

(a) Phase diagram - Number of phases conventional algorithm

(b) Total NR iterations - conventional algorithm

(c) Total SS iterations - conventional algorithm

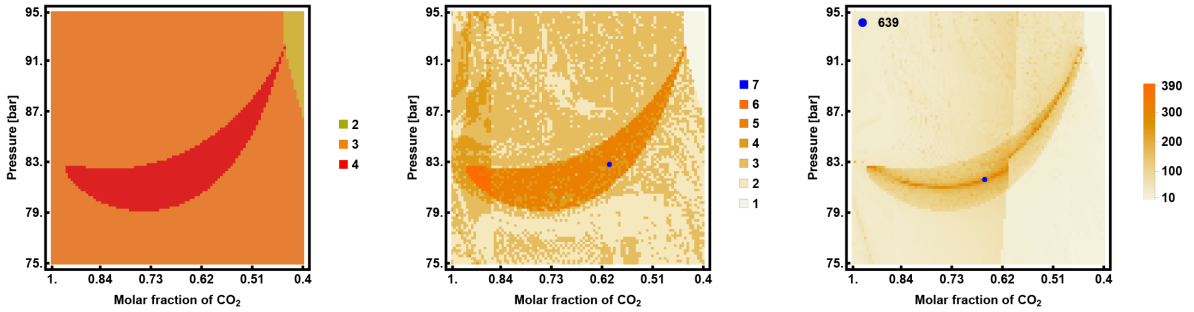

(d) Phase diagram - Number of phases improved algorithm

(e) Total NR iterations - improved algorithm

(f) Total SS iterations - improved algorithm

Fig. 2—Phase diagram and the total number of iterations in the conventional and improved algorithm: (a) phase diagram from the conventional algorithm, (b) total number of NR iterations from the conventional algorithm, (c) total number of SS iterations from the conventional algorithm, (d) phase diagram from the improved algorithm, (e) total number of NR iterations from the improved algorithm, and (f) total number of SS iterations from the improved algorithm. Example 1, BSB oil, eight-component mixture of H_2S, CO_2, and various hydrocarbons (Imai et al. 2019) at constant temperature T = 313.71 K.

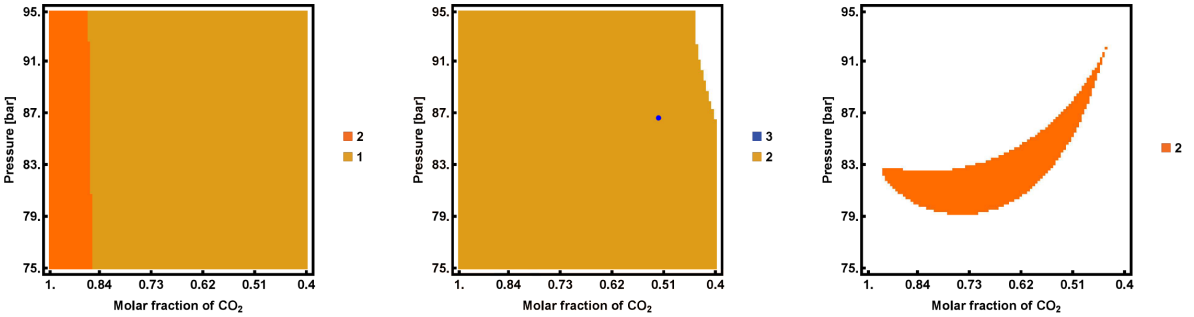

(a) 2 phase - Conventional algorithm

(b) 3 phase - Conventional algorithm

(c) 4 phase - Conventional algorithm

(d) 2 phase - Improved algorithm

(e) 3 phase - Improved algorithm

(f) 4 phase - Improved algorithm

Fig. 3—Number of NR iterations in the (a) conventional algorithm in two-phase split, (b) conventional algorithm in three-phase split, (c) conventional algorithm in four-phase split, (d) improved algorithm in two-phase split, (e) improved algorithm in three-phase split, and (f) improved algorithm in four-phase split. Example 1, BSB oil, eight-component mixture of H_2S, CO_2, and various hydrocarbons (Imai et al. 2019) at constant temperature T = 313.71 K.

Example 2: Four-Phase Split. In the second example, the stability and phase composition of a five-component mixture from Paterson et al. (2018) is performed in 40,000 independent phase-split calculations. The physical properties of components in the mixture are presented in **Table 2.** The mixture is investigated in a 200 × 200 grid for the temperature T in the range of 130–150 K and the pressure P in the range of 1–10 bar. The phase state and the total number of iterations of the improved algorithm are presented in **Fig. 5.** In **Fig. 6,** we present the total number of iterations in two-, three-, and four-phase-split calculations from the improved algorithm.

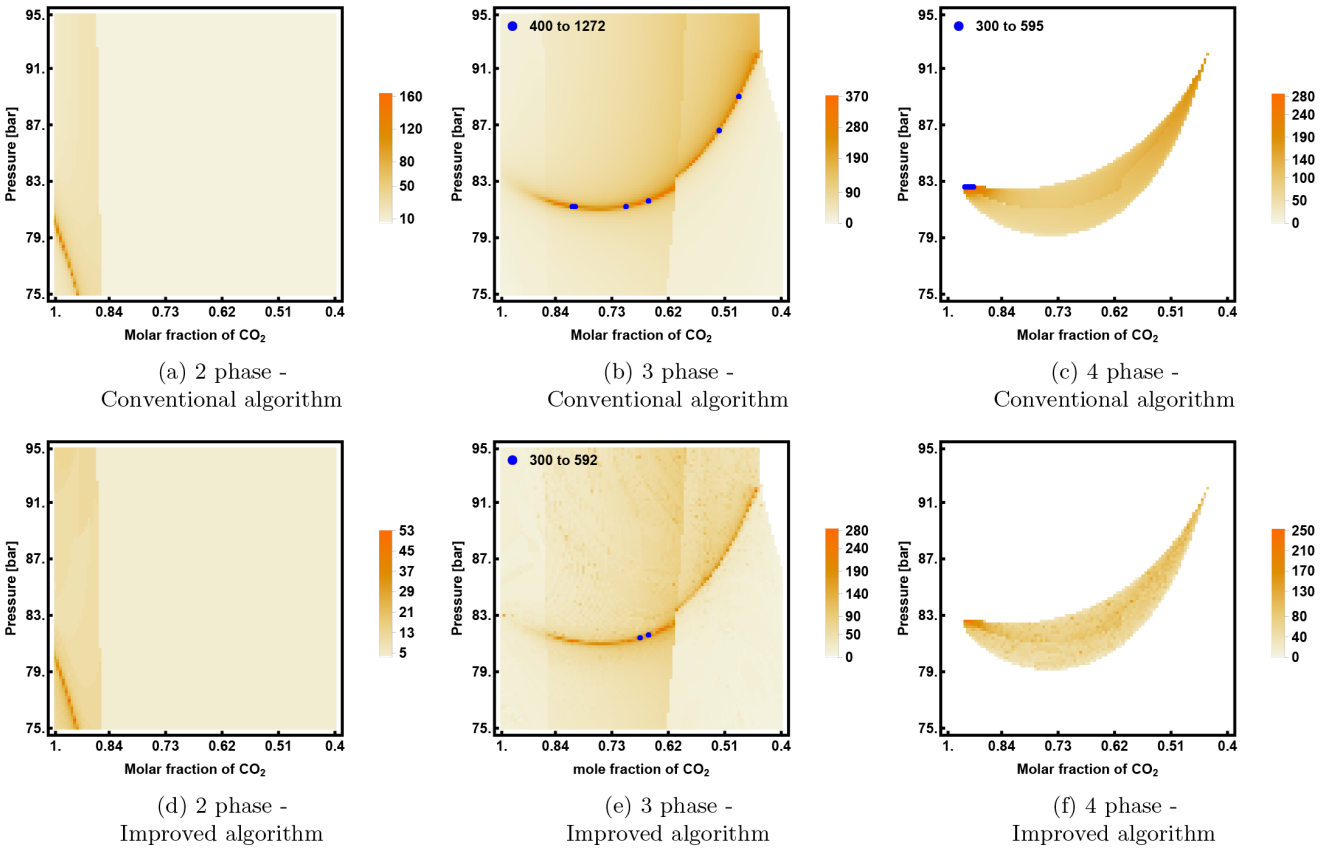

(a) 2 phase - Conventional algorithm
(b) 3 phase - Conventional algorithm
(c) 4 phase - Conventional algorithm
(d) 2 phase - Improved algorithm
(e) 3 phase - Improved algorithm
(f) 4 phase - Improved algorithm

Fig. 4—Number of SS iterations in the (a) conventional algorithm in two-phase split, (b) conventional algorithm in three-phase split, (c) conventional algorithm in four-phase split, (d) improved algorithm in two-phase split, (e) improved algorithm in three-phase split, (f) improved algorithm in four-phase split. Example 1, BSB oil, eight-component mixture of H_2S, CO_2, and various hydrocarbons (Imai et al. 2019) at constant temperature T = 313.71 K.

Components	T_c (K)	P_c (bar)	ω	CO_2 k_{il}	H_2S k_{il}	x_i^*
Methane (C_1)	190.56	45.99	0.0115	0.12	0.08	0.66
Ethane (C_2)	305.32	48.72	0.0995	0.15	0.07	0.03
Propane (C_3)	369.83	42.479	0.1523	0.15	0.07	0.01
Carbon dioxide (CO_2)	304.12	73.37	0.225	0.0	0.12	0.05
Hydrogen sulfide (H_2S)	373.1	90.0	0.10	0.12	0.0	0.25

Table 2—Relevant physical parameters and data: Example 2.

Example 3: Four-Phase Split. In the third example, the stability and phase composition of an eight-component mixture (JEMA oil plus water and carbon dioxide) from Imai et al. (2019) are performed with a total of 10,000 independent phase-split calculations. The physical properties of components in the mixture are presented in **Table 3.** The mixture is investigated in a 100 × 100 grid for the mixing molar fraction of CO_2 in the range of 0.4–0.9 and pressure P in the range of 80–90 bar and temperature of 316.48 K. Total numbers of iterations and number of phases are shown in **Fig. 7.** In **Fig. 8**, we present SS iterations in two-, three-, and four-phase-split calculations. In this mixture, we observe a higher number of iterations in three- and four-phase splits. In three-phase split, the region with a higher number of SS iterations is along the line in the middle of the four-phase envelope (see **Fig. 8e**). In four-phase split **(Fig. 8f)**, the region with a high number of SS iterations is on the top left of the four-phase envelope. **Fig. 7c** shows a high number of iterations in the SS even in the improved algorithm similar to **Fig. 2c**.

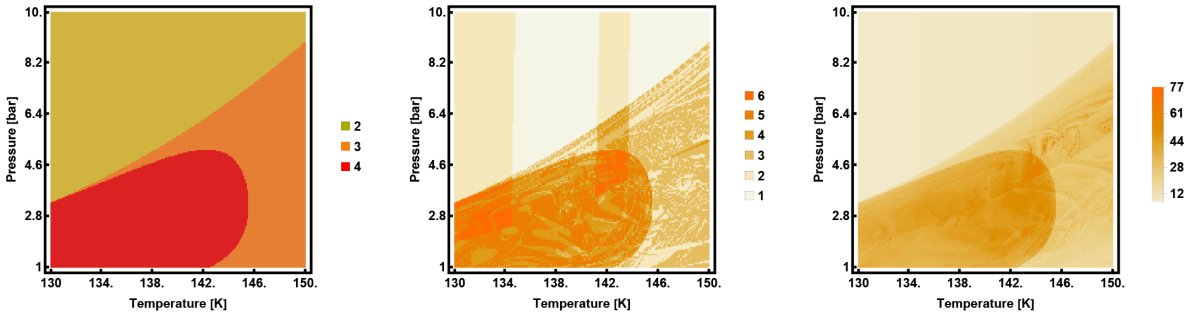

(a) Phase diagram - Number of phases (b) Total NR iterations (c) Total SS iterations

Fig. 5—Phase diagram and the total number of iterations in the improved algorithm: (a) number of phases, (b) total number of NR iterations, and (c) total number of SS iterations. Example 2, six-component mixture of C_1, C_2, C_3, H_2S, and CO_2 (Paterson et al. 2018).

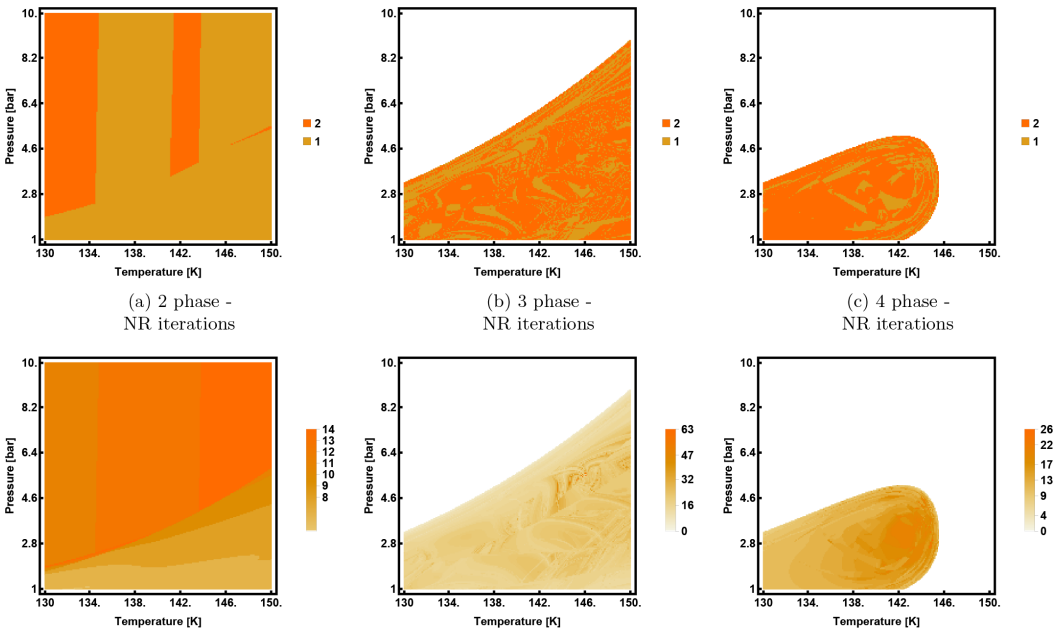

(a) 2 phase - NR iterations (b) 3 phase - NR iterations (c) 4 phase - NR iterations

(d) 2 phase - SS iterations (e) 3 phase - SS iterations (f) 4 phase - SS iterations

Fig. 6—Number of iterations in the improved algorithm: (a) NR in two-phase split, (b) NR in three-phase split, (c) NR in four-phase split, (d) SS in two-phase split, (e) SS in three-phase split, and (f) SS in four-phase split. Example 2, six-component mixture of C_1, C_2, C_3, H_2S, and CO_2 (Paterson et al. 2018).

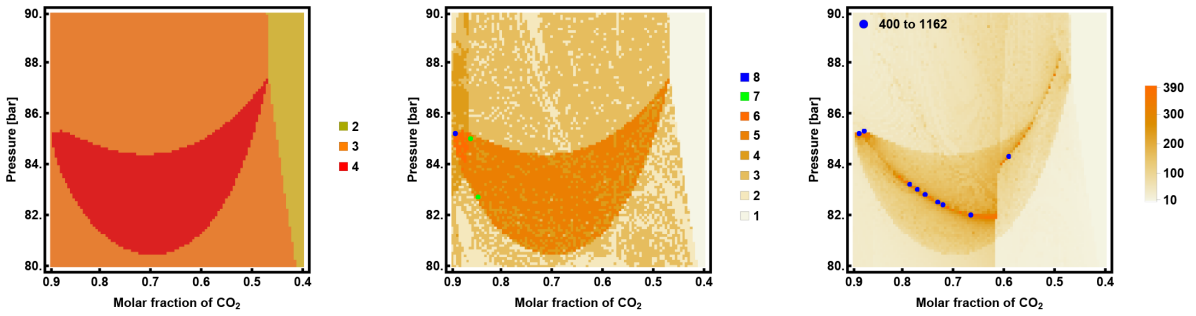

(a) Phase diagram - Number of phases (b) Total NR iterations (c) Total SS iterations

Fig. 7—Phase diagram and the total number of iterations in the improved algorithm: (a) number of phases, (b) total number of NR iterations, and (c) total number of SS iterations. Example 3, JEMA oil, eight-component mixture of H_2S, CO_2, and various hydrocarbons (Imai et al. 2019) at constant temperature T = 316.48 K.

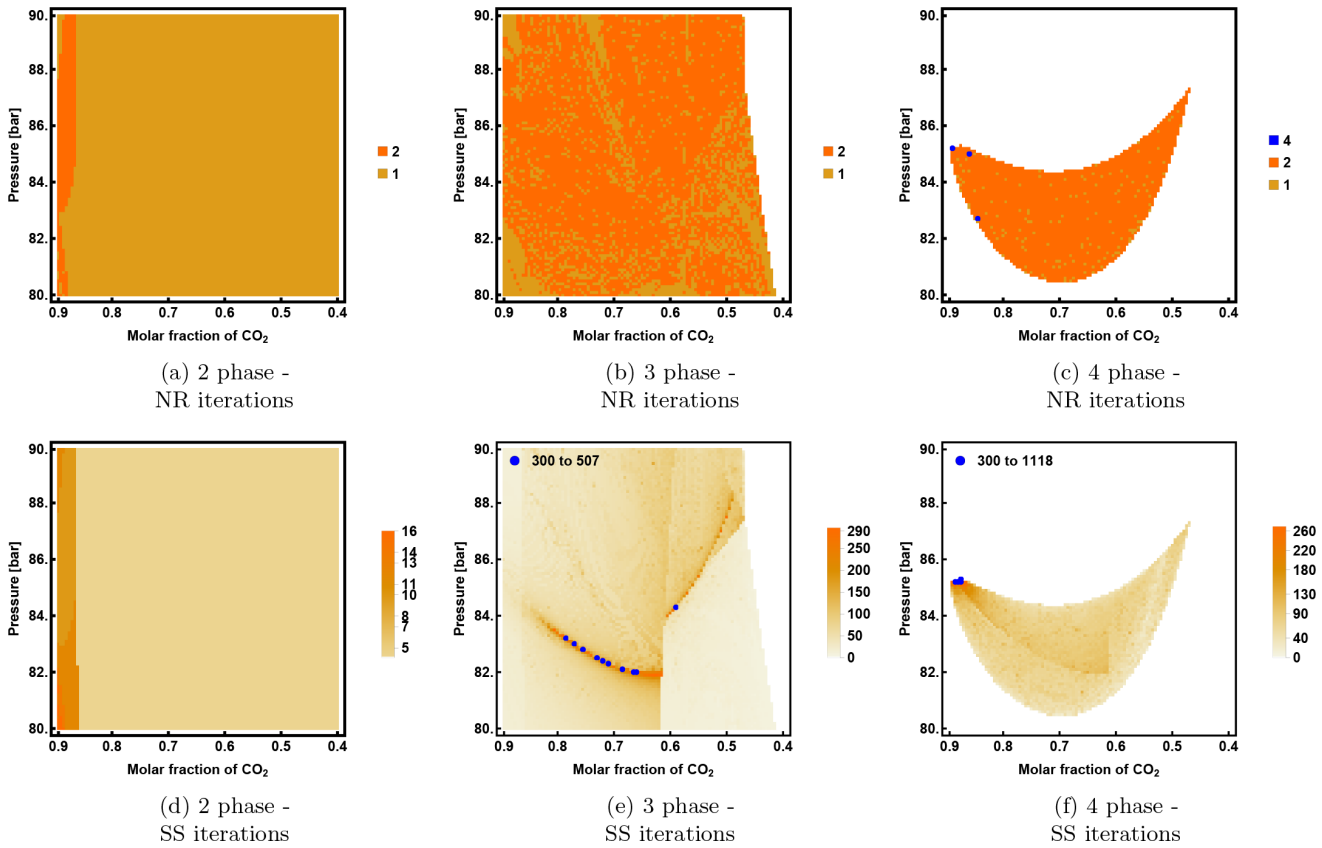

(a) 2 phase - NR iterations (b) 3 phase - NR iterations (c) 4 phase - NR iterations

(d) 2 phase - SS iterations (e) 3 phase - SS iterations (f) 4 phase - SS iterations

Fig. 8—Number of iterations in the improved algorithm: (a) NR in two-phase split, (b) NR in three-phase split, (c) NR in four-phase split, (d) SS in two-phase split, (e) SS in three-phase split, and (f) SS in four-phase split. Example 3, JEMA oil, eight-component mixture of H_2S, CO_2, and various hydrocarbons (Imai et al. 2019) at constant temperature T = 316.48 K.

Component	T_c (K)	P_c (bar)	ω	CO_2 k_{il}	H_2O k_{il}	x_i^*
H_2O	647.30	220.89	0.3440	0.095	0.0	0.3000
CO_2	304.20	73.76	0.2250	0.0	0.095	0.0134
C_1	166.67	46.00	0.0080	0.05	0.45	0.0485
C_{2-3}	338.81	45.53	0.1260	0.05	0.5	0.1219
C_{4-6}	466.12	33.68	0.2439	0.05	0.5	0.1361
C_{7-16}	611.11	20.95	0.6386	0.09	0.5	0.2197
C_{17-29}	777.78	15.88	1.0002	0.09	0.5	0.1084
C_{30+}	972.22	15.84	1.2812	0.09	0.5	0.0519

Table 3—Relevant physical parameters and data: Example 3.

Example 4: Three-Phase Split. The stability and phase composition of a seven-component mixture (NWE oil) from Chen et al. (2023) is performed with a total of 10,000 independent phase-split calculations. The physical properties of components are presented in **Table 4.** The mixture is investigated in a 100 × 100 grid for the mixing molar fraction in the range of 0–1 (of 0.95 mol CO_2 and 0.05 mol C_1) and pressure P in the range of 40–180 bar and T = 301.48 K. The total number of iterations and the number of phases are presented in **Fig. 9.** In **Fig. 10**, we present the number of iterations to conduct two- and three-phase-split calculations. We observe a similar iteration behavior to Examples 1–3, with the exception of two-phase split **(Fig. 10c)** in the middle of the three-phase envelope and in the three-phase split **(Fig. 10d)** on the top of the three-phase envelope.

Example 5: Three-Phase Split. In the fifth example, the stability and phase composition of a four-component mixture (BSB oil) from Chen et al. (2023) is performed with a total of 10,000 independent phase-split calculations. The physical properties of components in the mixture are presented in **Table 5.** The mixture is investigated in a 100 × 100 grid for the mixing molar fraction of CO_2 (0.95 mol CO_2 and 0.05 mol C_1) in the range of 0–1 and pressure P in the range of 20–160 bar and temperature T = 313.71 K. The total number of iterations and the number of phases are presented in **Fig. 11.** In **Fig. 12**, we present iterations in two- and three-phase-split calculations. The high

Component	T_c (K)	P_c (bar)	ω	CO_2 k_{il}	x_i^*
CO_2	304.20	73.76	0.225	0.0	0.0169
C_1	174.444	46.00	0.008	0.085	0.1752
C_{2-3}	347.263	44.69	0.133	0.085	0.2244
C_{4-6}	459.74	34.18	0.236	0.085	0.1673
C_{7-14}	595.135	21.87	0.598	0.104	0.2422
C_{15-25}	729.981	16.04	0.912	0.104	0.1216
C_{26+}	910.183	15.21	1.244	0.104	0.0524

Table 4—Relevant physical parameters and data: Example 4.

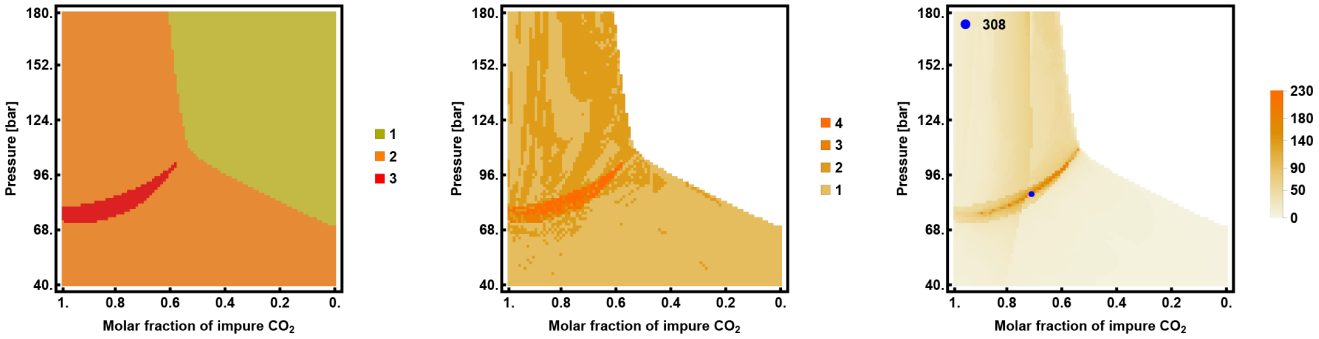

(a) Phase diagram - Number of phases (b) Total NR iterations (c) Total SS iterations

Fig. 9—Phase diagram and the total number of iterations in the improved algorithm: (a) number of phases, (b) total number of NR iterations, and (c) total number of SS iterations. Example 4, NWE oil, seven-component mixture of CO_2 and various hydrocarbons (Chen et al. 2023) at constant temperature T = 301.48 K.

number of iterations is in two-phase split **(Fig. 12c)** in the middle of the three-phase envelope, the same as in Example 3 **(Fig. 10)**, but in three-phase split **(Fig. 12d)**, the high number of iterations is in the left side of the three-phase envelope.

Substance	T_c (K)	P_c (bar)	ω	CO_2 k_{il}	x_i^*
CO_2	304.20	73.76	0.225	0.0	0.0169
C_1	160.00	46.00	0.008	0.055	0.1752
PC_1	529.03	27.32	0.481	0.081	0.6478
PC_2	795.33	17.31	1.042	0.090	0.2324

Table 5—Relevant physical parameters and data: Example 5.

In addition to the five examples above, we have also investigated the phase split in three other mixtures which are presented in Sections S-5, S-6, and S-7 of the Supplementary Material. Next, we present a detailed analysis of the SS and demonstrate the effectiveness of our modification.

Excessive Number of SS Iterations

In the past, it has been reported that the SS procedure may not converge to the minimum of Gibbs free energy (Heidemann and Michelsen 1995). The SS may even diverge when the initial guesses are close to the solution (Heidemann and Michelsen 1995). The report of very slow convergence and divergence is very limited over a wide range of PT and Pc spaces. In this work, we investigate a broad range of spaces. We observe a large number of iterations in the middle of the phase envelope away from the critical point and phase boundaries. The results in Petitfrere and Nichita (2014) also indicate increased iterations of both NR and trust region methods in two- and

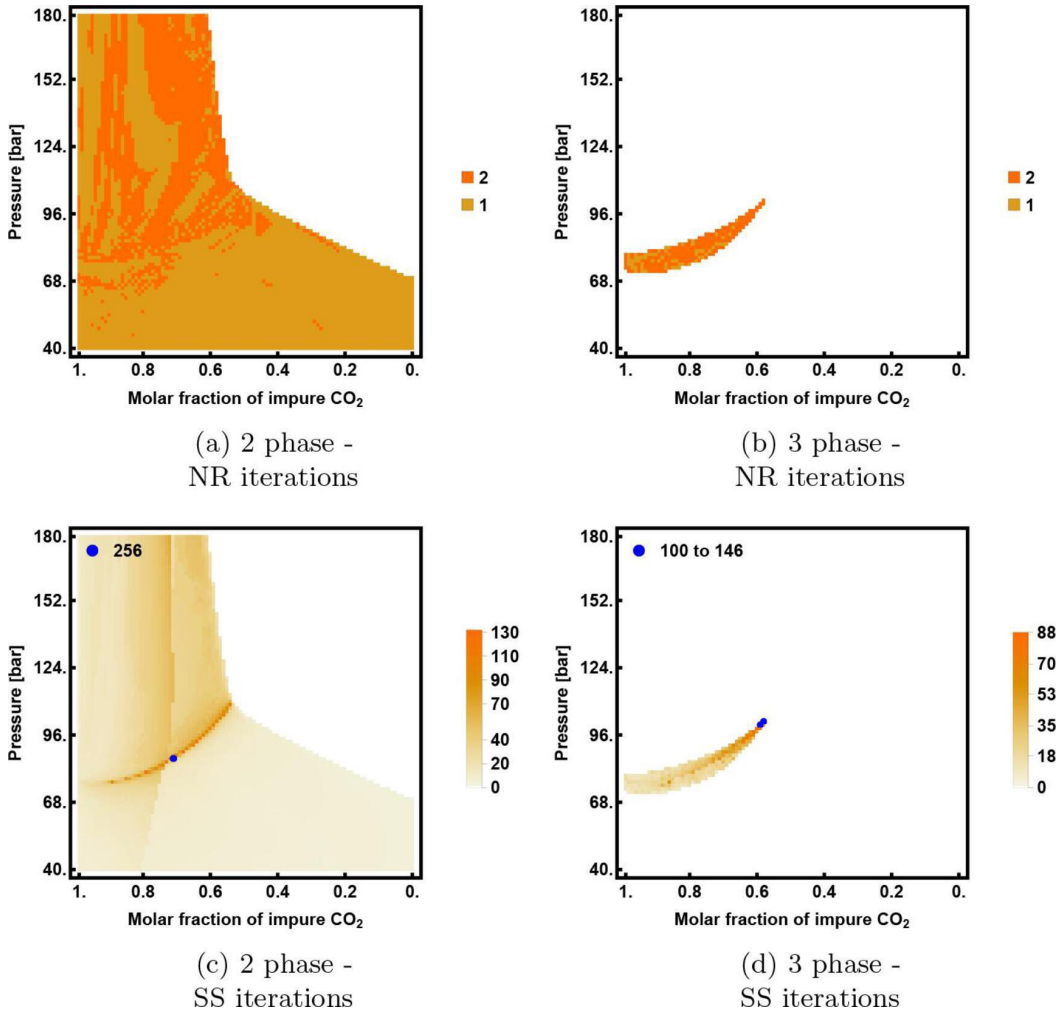

Fig. 10—Number of iterations in the improved algorithm: (a) NR in two-phase split, (b) NR in three-phase split, (c) SS in two-phase split, and (d) SS in three-phase split. Example 4, NWE oil, seven-component mixture of CO_2, and various hydrocarbons (Chen et al. 2023) at constant temperature T = 301.48 K.

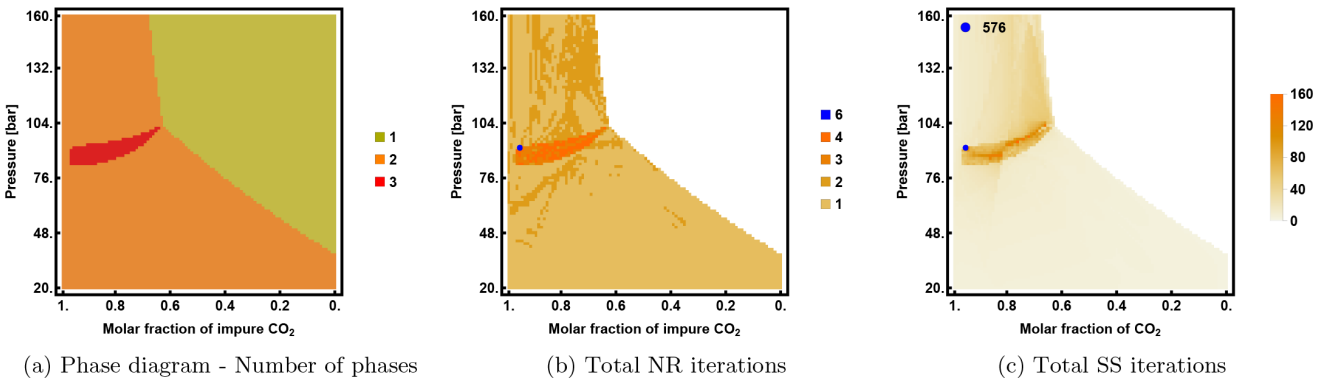

Fig. 11—Phase diagram and the total number of iterations in the improved algorithm: (a) number of phases, (b) cumulative number of NR iterations, and (c) cumulative number of SS iterations. Example 5, BSB oil, four-component mixture of CO_2, C_1, PC_1, and PC_2 (Chen et al. 2023) at constant temperature T = 313.71 K.

three-phase-split calculations in some regions, far from the critical point and the phase boundary. The number of iterations in the NR and trust region methods by Petitfrere and Nichita (2014) ranges from 4 to about 50. The trust region method, a Newton-type method, has a higher CPU cost than the NR method in every iteration. Our results indicate that, with the improved implementation of the SS method, NR converges in one or two iterations in the vast majority of cases. In the following, we include examples with large numbers of iterations and show the effectiveness of our proposal on increasing the computational speed in multiphase-split calculations.

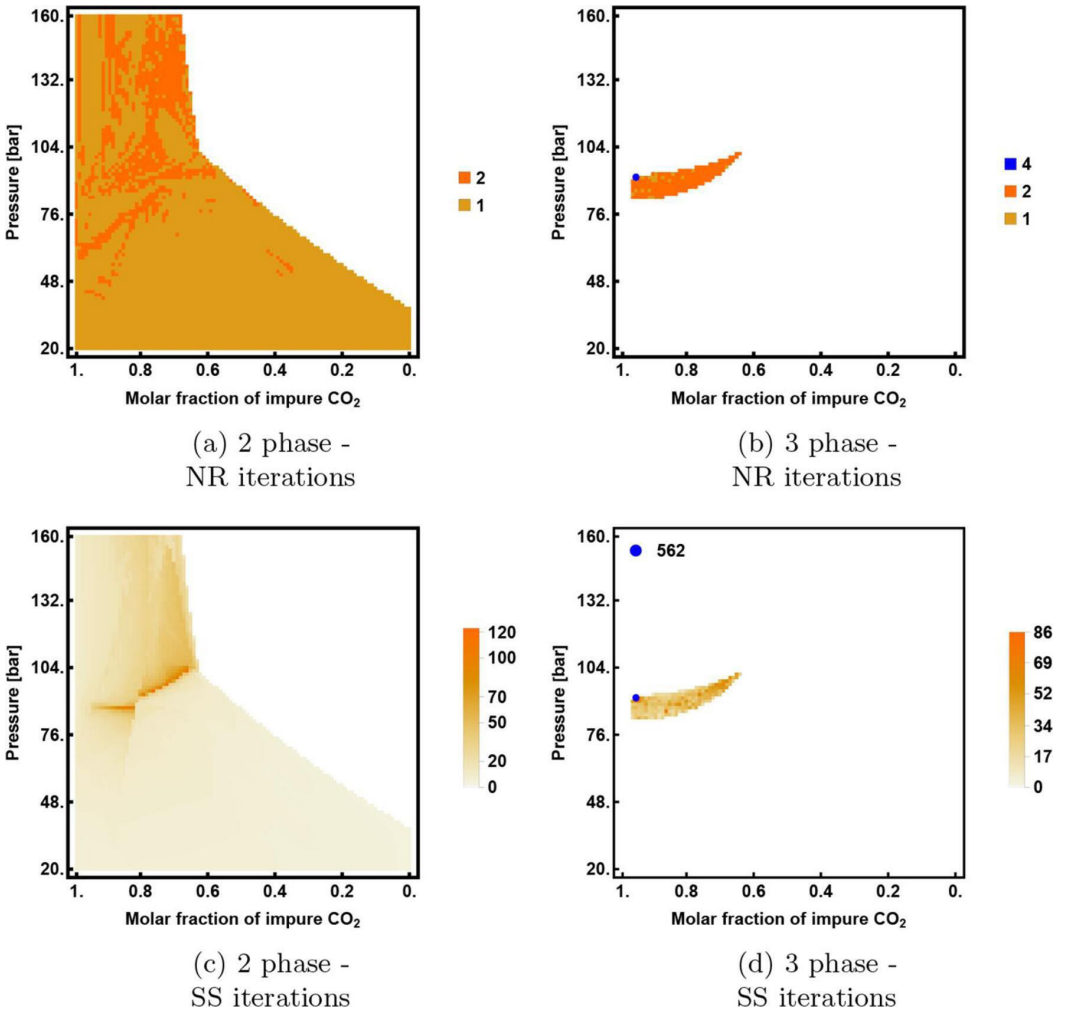

Fig. 12—Number of iterations in the improved algorithm: (a) NR in two-phase split, (b) NR in three-phase split, (c) SS in two-phase split, and (d) SS in three-phase split. Example 5, BSB oil, four-component mixture of CO_2, C_1, PC_1, and PC_2 (Chen et al. 2023) at constant temperature T = 313.71 K.

JEMA Sample. One of the high iteration cases is Example 3, JEMA mixture at P = 82 bar and molar mixing fraction of CO_2 of 0.65. Under these conditions, the mixture is in three-phase state. **Figs. 13 and 14** show the evolution of K values and ΔG in the SS iterations. **Fig. 13a** shows that convergence is fast once the step size parameter $\mathbf{m}^{(k)}$ is applied in Eq. 12 from Eq. 13. There is a significant reduction in the number of iterations to reach the assigned convergence criteria. **Fig. 15** shows that the fluctuations in the Gibbs free energy decrease become less pronounced as we reduce the step size from the predictions in Eq. 13. The maximum step size in Eq. 13 is 20. We use step sizes from 1 to 20 in the calculations in **Fig. 15a**. An observation relates to the nonmonotonous change of phase molar fraction ν_1 (1 is the phase index) and the compressibility factor of Phase 1 and selected equilibrium ratios (K values). The effect of different approaches to limit parameter $\mathbf{m}^{(k)}$ on convergence is shown in **Fig. 15**.

Oil Sample 1. Oil Sample 1 at P = 240 bar and T = 629 K of Example 6 has high SS iterations in two-phase state. **Fig. 16** shows the evolution of several quantities during the SS iterations. Note the nonmonotonous behavior in some of the variables. The effect of different restrictions to limit parameter $\mathbf{m}^{(k)}$ on convergence is shown in **Fig. 17.** The start of acceleration based on the criteria is early. Despite a relatively pronounced fluctuation, there is very rapid convergence based on the step size from Eq. 13. As we limit the step size parameter to a larger extent, there is less fluctuation, but the convergence becomes slow.

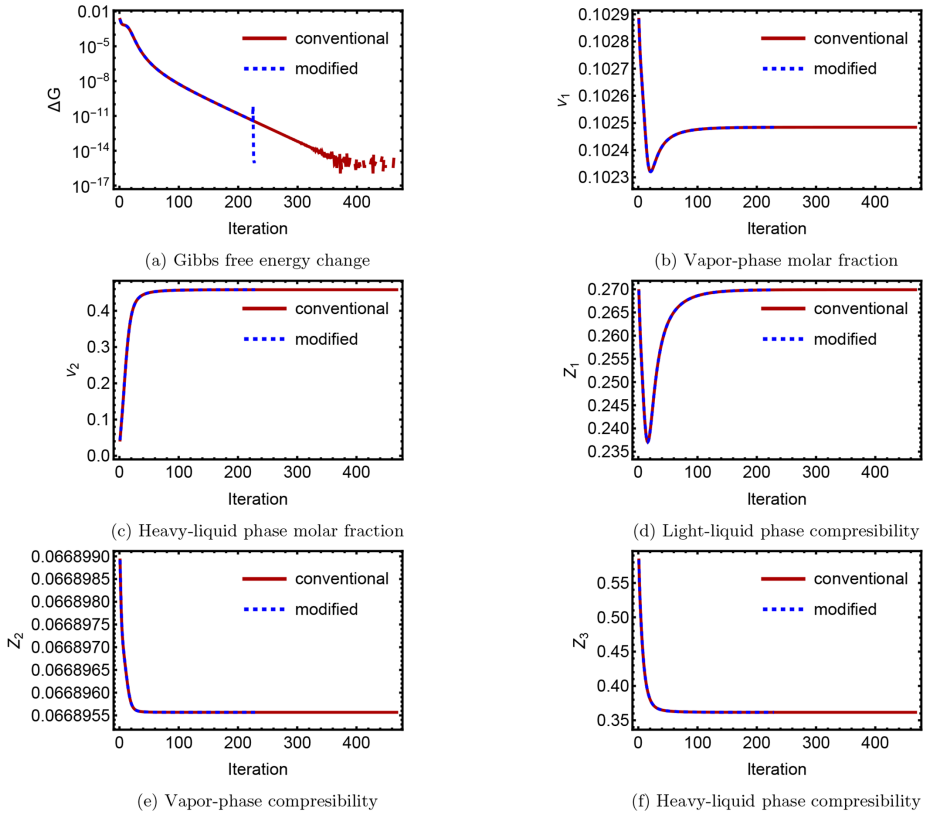

(a) Gibbs free energy change

(b) Vapor-phase molar fraction

(c) Heavy-liquid phase molar fraction

(d) Light-liquid phase compresibility

(e) Vapor-phase compresibility

(f) Heavy-liquid phase compresibility

Fig. 13—Evolution of various functions and parameters in three-phase split in the conventional and modified SS iterations: (a) Gibbs free energy change, (b) vapor-phase molar fraction v_1, (c) heavy liquid-phase molar fraction v_2, (d) light liquid-phase compressibility, (e) vapor-phase compressibility, and (f) heavy liquid-phase compressibility. Example 3, JEMA mixture at *P* = 82 bar and molar mixing fraction of 0.65 for CO_2.

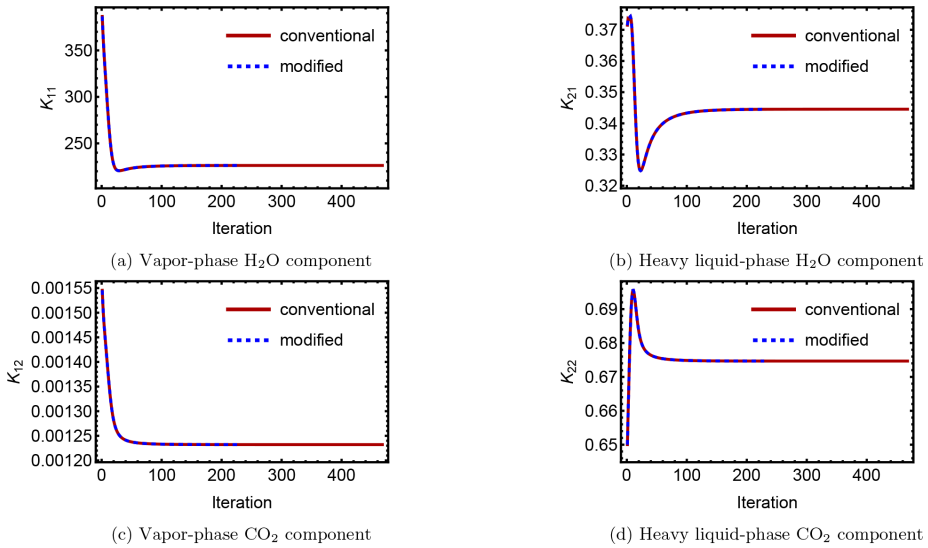

(a) Vapor-phase H_2O component

(b) Heavy liquid-phase H_2O component

(c) Vapor-phase CO_2 component

(d) Heavy liquid-phase CO_2 component

Fig. 14—Evolution of equilibrium ratios in three-phase split in the conventional and modified SS iterations: (a) vapor-phase H_2O component, (b) heavy liquid-phase H_2O component, (c) vapor-phase CO_2 component, and (d) heavy liquid-phase CO_2 component. Example 3, JEMA mixture at *P* = 2 bar and mixing fraction of 0.65 for CO_2.

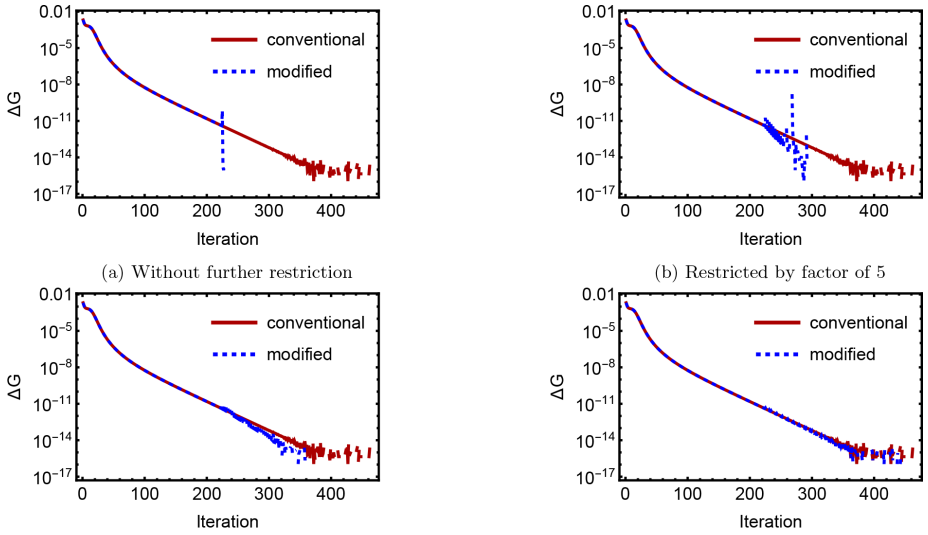

(a) Without further restriction

(b) Restricted by factor of 5

(c) Restricted by a factor of 2

(d) Restricted by a factor of 1.2

Fig. 15—Evolution of the Gibbs free energy decrease with limited step size in the conventional and modified SS iterations: (a) without further restriction, (b) maximum increase in step size restricted by a factor of 5, (c) maximum increase in step size restricted by a factor of 2, and (d) maximum step size increase restricted by a factor of 1.2. Example 3, JEMA mixture at P = 82 bar and mixing molar fraction of 0.65 for CO_2.

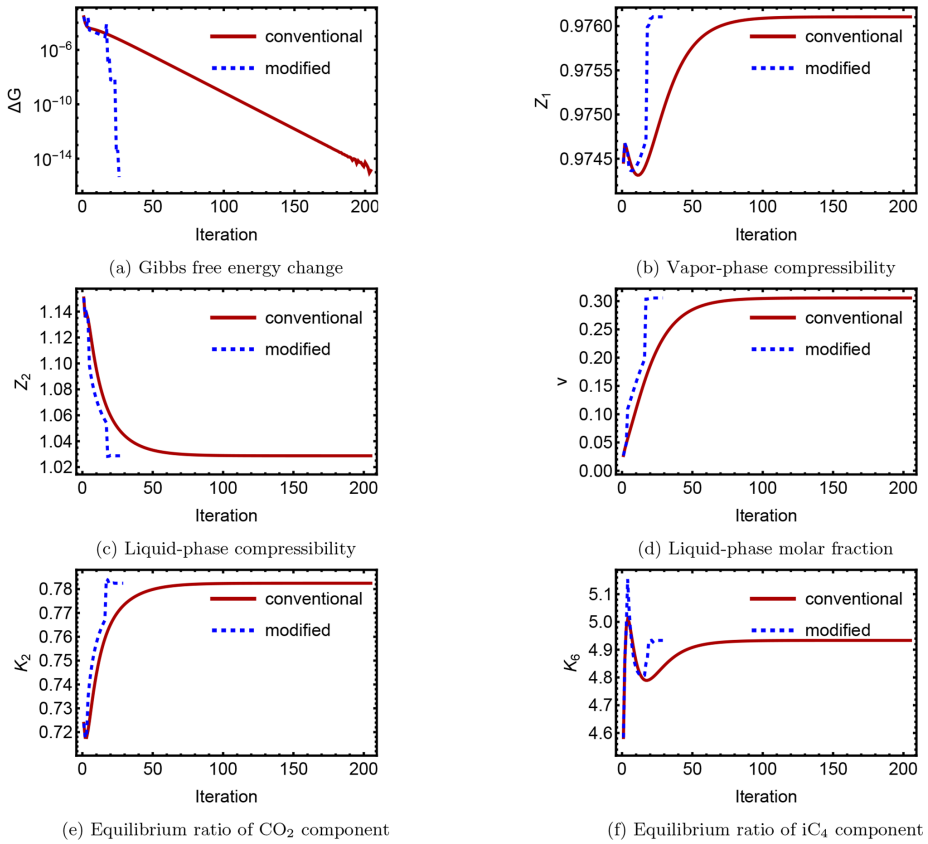

(a) Gibbs free energy change

(b) Vapor-phase compressibility

(c) Liquid-phase compressibility

(d) Liquid-phase molar fraction

(e) Equilibrium ratio of CO_2 component

(f) Equilibrium ratio of iC_4 component

Fig. 16—Evolution of various functions and parameters in two-phase split in the conventional and modified SS iterations: (a) Gibbs free energy change, (b) vapor-phase compressibility, (c) liquid-phase compressibility, (d) liquid-phase molar fraction v, (e) equilibrium ratio of CO_2 component, and (f) equilibrium ratio of iC_4 component. Example 6, Oil Sample 1 mixture at P = 240 bar and T = 629 K.

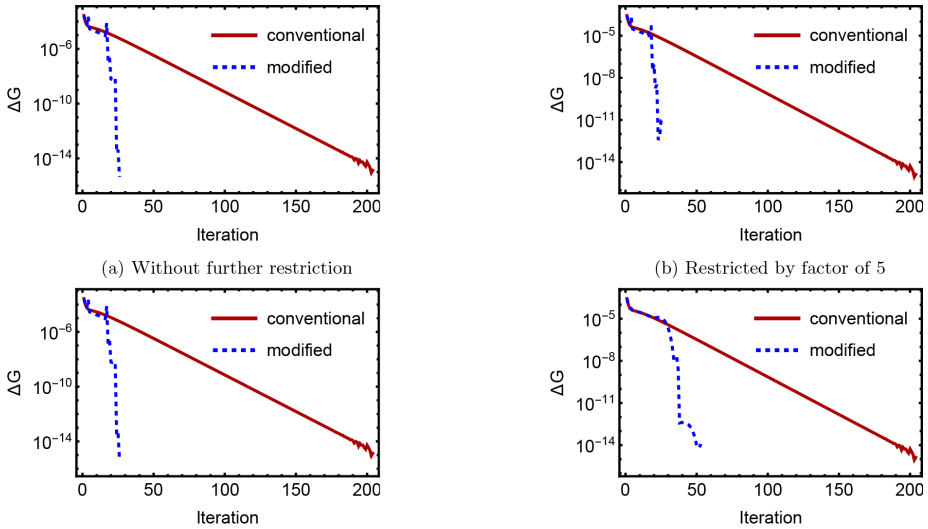

Fig. 17—Evolution of the Gibbs free energy decrease with limited step size in the conventional and modified SS iterations: (a) without further restriction, (b) maximum increase in step size restricted by a factor of 5, (c) maximum increase in step size restricted by a factor of 2, and (d) maximum step size increase restricted by a factor of 1.2. Example 6, Oil Sample 1 mixture at *P* = 240 bar and *T* = 629 K.

Two other examples of slow convergence and the speedup from the step size factor from Eq. 13 are presented in Sections S-2 and S-3 of the Supplementary Material.

Conclusions

A fully robust algorithm is introduced to perform two-, three-, and four-phase-split calculations efficiently. Eight different mixtures over a wide range of pressure, temperature, and composition space are investigated in some 150,000 independent phase stability and phase-split calculations. There is convergence in all calculations. The focus of the work is on phase-split calculations. In our work, we adapt the conventional approach of phase stability followed by phase-split calculations. In phase split into two, three, and four phases, the SS provides the initial guess for the NR method. In our algorithm, NR usually converges in one or two iterations in two-, three-, and four-phase splits. Although the SS iterations always converge, the convergence can be very slow, in some cases in thousands of iterations. In the past, slow convergence has been reported widely in the critical region and close to phase boundaries. Four-phase-split calculations have been reported to have more issues than two- and three-phase-split calculations. In this work, we find that, in the middle of the phase envelope, there may also be a region of very slow convergence in the SS method. We extend the acceleration of SS presented in the past from two to three and four phases. We also examine the Gibbs free energy change toward the minimum. A criterion is presented to speed up the SS. There is a significant reduction in the number of iterations in two-, three-, and four-phase-split calculations. In 150,000 independent phase-split computations, we observe robustness and efficiency.

Acknowledgments

Martin Jex and Jiří Mikyška have been supported by the Czech Science Foundation Project No. 21-09093S and Grant No. SGS23/188/OHK4/3 T/14 of the Grant Agency of the Czech Technical University in Prague. Abbas Firoozabadi is supported by the RERI Research Consortium.

References

Chen, Z., Xu, L., Zhou, Y. et al. 2023. A Robust and Efficient Algorithm for Vapor-Liquid-Equilibrium/Liquid-Liquid-Equilibrium (VLE/LLE) Phase Boundary Tracking. *Chem Eng Sci* **266**: 118286. https://doi.org/10.1016/j.ces.2022.118286.

Connolly, M., Pan, H., and Tchelepi, H. 2019. Three-Phase Equilibrium Computations for Hydrocarbon–Water Mixtures Using a Reduced Variables Method. *Ind Eng Chem Res* **58** (32): 14954–14974. https://doi.org/10.1021/acs.iecr.9b00695.

Firoozabadi, A. 2016. *Multiphase Flow and Transport Processes in the Subsurface, A Contribution to the Modelling of Hydrosystems*. New York, New York, USA: McGraw-Hill Education.

Heidemann, R. A. and Michelsen, M. L. 1995. Instability of Successive Substitution. *Ind Eng Chem Res* **34** (3): 958–966. https://doi.org/10.1021/ie00042a032.

Hoteit, H. and Firoozabadi, A. 2006. Simple Phase Stability-testing Algorithm in the Reduction Method. *AIChE J* **52** (8): 2909–2920. https://doi.org/10.1002/aic.10908.

Imai, M., Pan, H., Connolly, M. et al. 2019. Reduced Variables Method for Four-Phase Equilibrium Calculations of Hydrocarbon-Water-CO_2 Mixtures at a Low Temperature. *Fluid Ph Equilib* **497**: 151–163. https://doi.org/10.1016/j.fluid.2019.06.002.

Li, Z. and Firoozabadi, A. 2012. General Strategy for Stability Testing and Phase-Split Calculation in Two and Three Phases. *SPE J.* **17** (4): 1096–1107. https://doi.org/10.2118/129844-PA.

Li, R. and Li, H. A. 2019. Improved Three-Phase Equilibrium Calculation Algorithm for Water/Hydrocarbon Mixtures. *Fuel* **244**: 517–527. https://doi.org/10.1016/j.fuel.2019.02.026.

Mehra, R. K., Heidemann, R. A., and Aziz, K. 1983. An Accelerated Successive Substitution Algorithm. *Can J Chem Eng* **61** (4): 590–596. https://doi.org/10.1002/cjce.5450610414.

Michelsen, M. L. 1982a. The Isothermal Flash Problem. Part I. Stability. *Fluid Ph Equilib* **9** (1): 1–19. https://doi.org/10.1016/0378-3812(82)85001-2.
Michelsen, M. L. 1982b. The Isothermal Flash Problem. Part II. Phase-Split Calculation. *Fluid Ph Equilib* **9** (1): 21–40. https://doi.org/10.1016/0378-3812(82)85002-4.
Michelsen, M. L. 1993. Phase Equilibrium Calculations. What Is Easy and What Is Difficult? *Comput Chem Eng* **17** (5–6): 431–439. https://doi.org/10.1016/0098-1354(93)80034-K.
Mikyška, J. 2023. Robust and Efficient Methods for Solving the Rachford–Rice Equation in Flash Equilibrium Calculation. *Fluid Ph Equilib* **571**: 113803. https://doi.org/10.1016/j.fluid.2023.113803.
Okuno, R., Johns, R. T., and Sepehrnoori, K. 2010. A New Algorithm for Rachford-Rice for Multiphase Compositional Simulation. *SPE J.* **15** (2): 313–325. https://doi.org/10.2118/117752-PA.
Pan, H., Connolly, M., and Tchelepi, H. 2019. Multiphase Equilibrium Calculation Framework for Compositional Simulation of CO_2 Injection in Low-Temperature Reservoirs. *Ind Eng Chem Res* **58** (5): 2052–2070. https://doi.org/10.1021/acs.iecr.8b05229.
Pan, H., Imai, M., Connolly, M. et al. 2021. Solution of Multiphase Rachford-Rice Equations by Trust Region Method in Compositional and Thermal Simulations. *J Pet Sci Eng* **200**: 108150. https://doi.org/10.1016/j.petrol.2020.108150.
Paterson, D., Michelsen, M. L., Yan, W. et al. 2018. Extension of Modified RAND to Multiphase Flash Specifications Based on State Functions Other than (T,P). *Fluid Ph Equilib* **458**: 288–299. https://doi.org/10.1016/j.fluid.2017.10.019.
Peng, D.-Y. and Robinson, D. B. 1976. A New Two-Constant Equation of State. *Ind Eng Chem Fund* **15** (1): 59–64. https://doi.org/10.1021/i160057a011.
Perschke, D. R. 1988. *Equation of State Phase Behavior Modeling for Compositional Simulation*. PhD Dissertation, The University of Texas at Austin, Austin, Texas, USA.
Petitfrere, M. and Nichita, D. V. 2014. Robust and Efficient Trust-Region Based Stability Analysis and Multiphase Flash Calculations. *Fluid Ph Equilib* **362**: 51–68. https://doi.org/10.1016/j.fluid.2013.08.039.
Petitfrere, M. and Nichita, D. V. 2015. Multiphase Equilibrium Calculations Using a Reduction Method. *Fluid Ph Equilib* **401**: 110–126. https://doi.org/10.1016/j.fluid.2015.05.006.
Rachford, H. H. and Rice, J. D. 1952. Procedure for Use of Electronic Digital Computers in Calculating Flash Vaporization Hydrocarbon Equilibrium. *J Pet Technol* **4** (10): 19–23. https://doi.org/10.2118/952327-G.
Risnes, R. 1981. Phase Equilibrium Calculations in the near Critical Region. In *Enhanced Oil Recovery: Proceedings of the Third European Symposium on Enhanced Oil Recovery, Held in Bournemouth, U.K., September 21-23, 1981*, ed. F. John Fayers, Chap. 21, 329–350. USA, Canada, North-Holland: Elsevier Scientific Pub. Co.
Shima, E., Ochi, A., Nakamura, T. et al. 1999. Unstructured Grid CFD On Numerical Wind Tunnel. In *Parallel Computational Fluid Dynamics 1998*, eds. C. Lin, A. Ecer, and J. Periaux. et al, 475–482. Amsterdam: North-Holland.
Trangenstein, J. A. 1987. Customized Minimization Techniques for Phase Equilibrium Computations in Reservoir Simulation. *Chem Eng Sci* **42** (12): 2847–2863. https://doi.org/10.1016/0009-2509(87)87051-3.